Late accretion on the earliest planetesimals revealed by the highly siderophile elements

Christopher W. Dale[1], Kevin W. Burton[1], Richard C. Greenwood[2], Abdelmouhcine Gannoun[3], Jonathan Wade[4], Bernard J. Wood[4], D. Graham Pearson[1,5]

[1] Department of Earth Sciences, Durham University, Durham, DH1 3LE, UK

[2] Planetary and Space Science Research Institute, Open University, Walton Hall, Milton Keynes, MK7 6AA, UK

[3] Laboratoire Magmas et Volcans, OPGC, UBP, UMR 6524, 5 Rue Kessler 63038 Clermont Ferrand cedex, France

[4] Department of Earth Sciences, University of Oxford, Parks Road, Oxford, OX1 3PR, UK

[5] Department for Earth and Atmospheric Sciences, University of Alberta, Edmonton, T6G 2E3, Canada

*To whom correspondence should be addressed. E-mail: christopher.dale@durham.ac.uk

Late accretion of primitive, chondritic material to Earth, the Moon and Mars, after core formation had ceased, can account for the absolute and relative abundances of highly siderophile elements (HSEs) in their silicate mantles. Here we show that smaller planetesimals also possess elevated HSE abundances in chondritic proportions. This demonstrates that late addition of chondritic material was a common feature of all differentiated planets and planetesimals irrespective of when they accreted; occurring ≤5 to ≥150 Myr after the formation of the solar system. Parent-body size played a role in producing variations in absolute HSE abundances amongst these bodies, however, the oxidation state of the body exerted the major control by influencing the extent to which late-accreted material was mixed into the silicate mantle rather than removed to the core.

Highly siderophile (iron-loving) elements (HSEs: Re, Os, Ir, Ru, Rh, Pt, Pd and Au) have low-pressure metal-silicate partition coefficients that are extremely high (10^7 to 10^{15}) (e.g. *1, 2*). Consequently, these elements should have been substantially partitioned into the metallic cores of the Earth, and other rocky planets, leaving their silicate mantles effectively stripped of HSEs. Yet the concentrations of the HSEs in the Earth's upper mantle (e.g. *3*) and the martian mantle (*4, 5*) are much greater than predicted from low pressure experimental data (Fig. 1 inset)(*6*). The siderophile behaviour of some

HSEs may, however, be greatly reduced under high pressure-temperature conditions, and on this basis it has been suggested that high-pressure equilibration at the base of a deep molten silicate layer, or 'magma ocean' (*7, 8*) may account for their abundances in Earth's mantle. Nevertheless, the large apparent range of partition coefficients for HSEs, even at the elevated temperatures accompanying higher pressures in larger bodies (*9-11*), is not consistent with the chondritic (i.e. primitive solar system) patterns of HSEs in both the terrestrial and martian mantles, and the similarities in absolute abundances between the two bodies (*12*). This strongly suggests that high-pressure equilibration was not the dominant process controlling their present concentrations.

The simplest explanation of both the absolute and relative abundances of HSEs in the terrestrial and martian mantles is the late accretion of chondritic material following core formation, with material being mixed into the mantle by convection (*13, 14*). Chondritic late addition of between 0.4 and 1% of the mass of the terrestrial and martian mantles (*12*) is permitted by current dynamical models of planetary accretion. However, the Moon poses a problem because, despite its smaller cross section and much weaker gravitational field, its HSE concentrations (*15, 16*) are markedly lower than predicted by a late accretion hypothesis (*12*). Stochastic late accretion offers a solution to this problem, with late-stage material provided by impactors drawn from a leftover planetesimal population dominated, in mass terms, by large bodies (*17*). With such a population, a limited number of massive random impacts can deliver proportionally more material to Earth and Mars than to the much smaller Moon.

The accretionary histories of Vesta and similar asteroids were different from those of the terrestrial planets and the Moon, which accreted over timescales of 30-140 Myr (*4, 18*). The smaller asteroids appear to have experienced rapid, efficient and relatively low-pressure metal-silicate equilibration during global scale melting (*19*) within the first few million years of the solar system, with a relatively short time window for late accretion between the end of core formation and crystallisation of the

magma ocean or crust (*18*). Given the short timescale, and a relative deficit of small planetesimals available to be accreted (*17, 20*), it is reasonable to predict that the silicate portions of these planetesimals possess extremely low HSE abundances, potentially with fractionated relative proportions reflecting equilibration during core formation, without substantial late addition of chondritic material.

Here we present HSE abundances and $^{187}Os/^{188}Os$ isotope data (*21*) for basaltic meteorites: the eucrites and diogenites [part of the howardite-eucrite-diogenite (HED) suite generally believed, and assumed here, to sample the asteroid 4 Vesta], anomalous eucrites [considered to be from distinct Vesta-like parent bodies on the basis of their oxygen isotope compositions (*22*)], angrites (from an unidentified parent body) and SNCs (believed to be from Mars).

Initial assessment of our data indicates that all the basaltic meteorites studied here have HSE inter-element ratios (and Os isotope ratios) approaching those of chondrites (Figs. 1a and S1), with some enrichment in Pt, Pd and Re. There is no evidence for the extreme mantle depletions of Pt and Ir expected to accompany low-pressure metal-silicate equilibration (*1, 6*). The widespread enrichment in Pt, Pd and Re reflects the incompatible behaviour of these elements during partial mantle melting (*23*); that is, these elements preferentially enter the basaltic melt, relative to the mantle source. Consequently, the absolute and relative abundance of HSEs in the basaltic meteorites studied here are not the same as those of their mantle source. On Earth, HSE abundances in igneous rocks co-vary with Mg content, and one approach that has been used to estimate HSE abundances in the mantles of other planets is to compare their HSE-MgO co-variations with that of Earth (e.g. *15, 16; SOM*). The implicit assumption is that the conditions and mineral phases involved in melting and fractional crystallisation are the same in all bodies. For eucrites and diogenites, however, both believed to be from Vesta, this approach yields very different estimates of HSE concentrations in their mantle source (Fig. S2). Given that the raw data indicate an approximately chondritic pattern (Fig. 1), an alternative

method is to use the relative compatibility of the HSEs themselves to determine their concentrations in the melt source. For example, platinum behaves as a moderately incompatible element during melting (entering the melt) whereas osmium is highly compatible (and is retained in the residual mantle or cumulate rocks) resulting in higher Pt, and lower Os contents in basaltic melts, relative to their mantle source (cf. *24*). Consequently, Pt/Os ratios in magmatic rocks from the Earth and all other parent bodies, define arrays that can be seen to evolve from inter-element ratios and abundances that closely match those of their melt sources (Fig. 2 and SOM (*23*)). The slope of a given array will depend on the HSE partition coefficients for that parent body, but the origin of the array (source composition) is independent of this parameter.

Highly siderophile element abundances estimated in this way demonstrate that the fractionated patterns preserved in these basaltic meteorites evolved from sources with inter-element ratios that are broadly chondritic (Figs. 1b and 2), consistent with their $^{187}Os/^{188}Os$ isotope compositions (Fig. S4, Table S1). These data confirm that excess HSE concentrations (with respect to equilibrium core-mantle partitioning) are a common feature of differentiated planets and asteroidal bodies in the inner solar system; apparent both in meteorite parent bodies formed within 2-3 Myr of the beginning of the solar system and large planets such as Earth where accretion may have continued for several hundred million years. Several of the samples contain evidence for late-stage meteoritic contamination and thus do not reflect the HSE contents of their source mantle (*25*), but these samples aside, a striking feature of the data is that while each of these different parent-bodies possesses chondritic relative proportions of HSEs, the absolute abundances vary considerably (Fig. 1b). The estimate for Vesta (13 samples, both eucrites and diogenites) is uniformly low compared to the angrite and Pasamonte parent-bodies which are at least an order of magnitude more HSE-rich (*26*).

The principal controls on the HSE abundances in the silicate parts of these bodies must be, firstly, the extent of initial segregation into the metallic core and secondly, the nature and timing of late

accretion. For differentiated asteroids, like Vesta and the angrite-parent body, early global-scale melting (*19*) facilitated rapid and efficient core formation, consistent with core segregation ages that range from 3-6 Myr after the start of the solar system (*18*). Furthermore, because the pressure at which metal and silicate equilibrated during core segregation on Vesta was much lower (<2GPa) than on Earth, Mars or the Moon, variable but almost complete depletion of the HSEs in the residual mantle would be expected at the end of core formation (*1, 27*). Although very low absolute abundances are observed for Vesta, indicating substantial removal to the metallic core, the relative proportions of HSEs are chondritic, consistent with late accretion. For Earth, Mars and Vesta, HSE abundances appear to relate to parent-body size (Fig. 3a), suggesting proportionally more late-accreted material in larger bodies (~0.6% of the mantle mass for Earth, ~0.4% for Mars, ~0.01% for Vesta). This suggests that the extent of HSE enrichment depends on the time interval after the end of core formation and before complete solidification of the magma ocean, during which late-accreted material could be added and mixed into the mantle. This time-window for addition depends on cooling rate and hence on the size of the parent body. For Mars and Earth, in accord with the higher levels of HSEs in their mantles, the period over which late impactors could be accreted and mixed into the upper mantle was much longer and differed in timing (some 20 Myr for Mars after early core formation (*4, 18*) and up to 100 Myr for Earth after the giant Moon-forming impact (*18*)). In addition, plate tectonics may have provided a means of mixing late-accreted material into the Earth's interior even after complete magma ocean and crust solidification, but early Earth HSE contents were still much higher than in Vesta and the Moon (*28*). For early planetesimals (Vesta, angrite-, Ibitira- and Pasamonte-parent bodies) core formation ceased between 3-6 Myr after the formation of the CAIs, with magmatic crystallisation no more than a few million years later (e.g. *18*) consistent with their lower HSE contents. Nevertheless, the angrite parent body and the Moon possess much higher and lower mantle HSE abundances, respectively, than might be expected on the simple basis of their sizes

(*29*). It is apparent, therefore, that factors other than size were important in controlling HSE abundances.

A much better co-variation exists between the HSE abundances of planets and meteorite parent bodies and their oxygen fugacities, than between HSE abundance and size (Fig. 3b). This observation suggests that in reduced bodies late-accreted metal was predominantly added to the core whereas in oxidised bodies, such as Mars, Earth and the angrite parent body, metal was substantially mixed into the mantle. This is a logical consequence of the higher ferric iron contents of oxidised bodies because ferric iron provides the potential for the oxidation of metal and its dissolution in mantle silicates (e.g. *6, 30*). During the principal phase of metallic core formation all bodies were saturated in metal and hence highly reduced. Oxidation is believed to have occurred through the addition of more oxidised materials towards the end of accretion (e.g. *31*). In the cases of Earth and Mars there was an additional mechanism for the production of ferric iron through the disproportionation of ferrous iron into ferric iron plus Fe-metal (*32, 33*). This mechanism requires the stabilisation of silicate perovskite at very high pressures in the lower mantle, a process which occurs widely on Earth, to a small extent on Mars and not at all in smaller bodies.

It appears that late accretion was spatially and temporally widespread in the inner solar system, with HSE abundances in differentiated asteroids and the terrestrial planets reflecting both the extent of initial removal into the metallic core and the proportion of material added by late accretion. If oxidation state exerted the dominant control on HSE abundances in the silicate mantles of all bodies, including the Moon, it follows then that the oxidising conditions of the silicate mantles of the Earth and Mars were established prior to, or synchronously with late accretion, although not necessarily at the conditions seen at the present-day.

Reference and Notes

1. A. Borisov, H. Palme, B. Spettel, Solubility of Palladium in Silicate Melts - Implications for Core Formation in the Earth. Geochimica Et Cosmochimica Acta 58, 705 (1994).

2. W. Ertel, H. S. O'Neill, P. J. Sylvester, D. B. Dingwell, Solubilities of Pt and Rh in a haplobasaltic silicate melt at 1300 degrees C. Geochimica Et Cosmochimica Acta 63, 2439 (1999).

3. H. Becker et al., Highly siderophile element composition of the Earth's primitive upper mantle: Constraints from new data on peridotite massifs and xenoliths. Geochimica et Cosmochimica Acta 70, 4528 (2006).

4. A. D. Brandon, R. J. Walker, J. W. Morgan, C. G. Goles, Re-Os isotopic evidence for early differentiation of the Martian mantle. Geochimica et Cosmochimica Acta 64, 4083 (2000).

5. J. H. Jones, C. R. Neal, J. C. Ely, Signatures of the highly siderophile elements in the SNC meteorites and Mars: a review and petrologic synthesis. Chemical Geology 196, 21 (2003).

6. K. Kimura, R. S. Lewis, E. Anders, Distribution of gold and rhenium between nickel-iron and silicate melts - Implications for abundance of siderophile elements on Earth and Moon. Geochimica et Cosmochimica Acta 38, 683 (1974).

7. K. Righter, M. Humayun, L. Danielson, Partitioning of palladium at high pressures and temperatures during core formation. Nat. Geosci. 1, 321 (2008).

8. V. R. Murthy, Early Differentiation of the Earth and the Problem of Mantle Siderophile Elements - a New Approach. Science 253, 303 (1991).

9. W. Ertel, M. J. Walter, M. J. Drake, P. J. Sylvester, Experimental study of platinum solubility in silicate melt to 14 GPa and 2273 K: Implications for accretion and core formation in Earth. Geochimica et Cosmochimica Acta 70, 2591 (2006).

10. J. M. Brenan, W. F. McDonough, Core formation and metal-silicate fractionation of osmium and iridium from gold. Nat. Geosci. 2, 798 (2009).

11. A. Holzheid, P. Sylvester, H. S. C. O'Neill, D. C. Rubie, H. Palme, Evidence for a late chondritic veneer in the Earth's mantle from high-pressure partitioning of palladium and platinum. Nature 406, 396 (2000).

12. R. J. Walker, Highly siderophile elements in the Earth, Moon and Mars: Update and implications for planetary accretion and differentiation. Chemie Der Erde-Geochemistry 69, 101 (2009).

13. C.-L. Chou, Fractionation of siderophile elements in the Earth's upper mantle, Lunar Planet. Sci. Conf. IX, 219-230 (1978).

14. Alternative models to explain the HSE contents of the silicate mantles of Earth, Mars and the Moon include reduced sequestering of HSE by metal at high temperatures and pressures, and inefficient core formation. The former scenario is not supported by current data. Furthermore, adequate convergence of partition coefficients for all HSE at high temperature and pressure seems unlikely. Inefficient core formation, whereby solid or liquid metal is retained in the mantle during core formation, can account for any given siderophile element concentration according to the precise proportion of solid and liquid metal retained. The differing compatibility of HSE in liquid and solid metal, however, will lead to HSE fractionation by this process. It is also difficult to account for the concentrations of other siderophile and chalcophile elements such as Ni, Co and S by any one set of parameters (12).

15. J. M. D. Day, D. G. Pearson, L. A. Taylor, Highly siderophile element constraints on accretion and differentiation of the Earth-Moon system. Science 315, 217 (2007).

16. J. M. D. Day, R. J. Walker, O. B. James, I. S. Puchtel, Osmium isotope and highly siderophile element systematics of the lunar crust. Earth and Planetary Science Letters 289, 595 (2010).

17. W. F. Bottke, R. J. Walker, J. M. D. Day, D. Nesvorny, L. Elkins-Tanton, Stochastic Late Accretion to Earth, the Moon, and Mars. Science 330, 1527 (2010).

18. T. Kleine et al., Hf-W chronology of the accretion and early evolution of asteroids and terrestrial planets. Geochimica et Cosmochimica Acta 73, 5150 (2009).

19. R. C. Greenwood, I. A. Franchi, A. Jambon, P. C. Buchanan, Widespread magma oceans on asteroidal bodies in the early Solar System. Nature 435, 916 (2005).

20. A. Morbidelli, W. F. Bottke, D. Nesvorny, H. F. Levison, Asteroids were born big. Icarus 204, 558 (2009).

21. Materials and methods are available in SOM; analyses were performed following techniques described previously.

22. E. R. D. Scott, R. C. Greenwood, I. A. Franchi, I. S. Sanders, Oxygen isotopic constraints on the origin and parent bodies of eucrites, diogenites, and howardites. Geochimica et Cosmochimica Acta 73, 5835 (2009).

23. There is less fractionation of Pt, Pd and Re from Os, Ir and Ru during partial mantle melting on Vesta and the Moon than on Earth (e.g. Fig. 2). This is most likely due to the differing oxygen and

sulphur fugacities on these PBs, which will affect partitioning of HSEs between mantle minerals and melts, and also, more importantly, affect the stability of phases which control the HSE budget. For example, metal exists at the oxygen fugacities present in the lunar and vestan mantles, but not in the Earth's upper mantle.

24. J. L. Birck, C. J. Allegre, Contrasting Re/Os magmatic fractionation in planetary basalts. Earth and Planetary Science Letters 124, 139 (1994).

25. After correction, some of the basaltic meteorite samples preserve very high HSE abundances, namely Johnstown (diogenite), Dhofar 007 (eucrite) and NWA2999 (angrite). It is possible that these high HSE concentrations reflect genuine abundances in the mantle of their parent body, implying substantial compositional heterogeneity. However, each of these meteorites contains an anomalously high proportion of metal (34,35; up to 10% for NWA2999), compared to <0.5% expected from equilibrium crystallisation (36), and has high Ni content, suggesting that each has been affected by impact-disturbance after, not before, igneous crystallisation. It is also notable that the actual measured HSE proportions in each of these samples are chondritic, with no inter-element variation that would be expected in either the residue or products of partial melting.

26. Previous data for HEDs suggested greater HSE heterogeneity in their parent body (37), but the relative uniformity of concentrations measured here suggests that at least some of that variation may be due to post-crystallisation meteoritic contamination. Inferred concentrations of HSEs in the angrite parent body are broadly consistent with previous angrite data (38).

27. A. Borisov, H. Palme, The solubility of iridium in silicate melts: New data from experiments with Ir10Pt90 alloys. Geochimica et Cosmochimica Acta 59, 481 (1995).

28. W. D. Maier et al., Progressive mixing of meteoritic veneer into the early Earth's deep mantle. Nature 460, 620 (2009).

29. It has been suggested that angrites were derived from a much larger body than inferred from the short timescale of core formation (18). While for the Moon it might be argued that if the lunar impactor, thought to make up ~80% of the Moon (e.g. 39 and references therein), was already differentiated and depleted then the formation of the lunar core may have further removed HSEs from its mantle.

30. D. J. Frost, U. Mann, Y. Asahara, D. C. Rubie, The redox state of the mantle during and just after core formation. Philosophical Transactions of the Royal Society A - Mathematical, Physical and Engineering Sciences 366, 4315 (2008).

31. F. Albarede, Volatile accretion history of the terrestrial planets and dynamic implications. Nature 461, 1227 (2009).

32. J. Wade, B. J. Wood, Core formation and the oxidation state of the Earth. Earth and Planetary Science Letters 236, 78 (2005).

33. D. J. Frost et al., Experimental evidence for the existence of iron-rich metal in the Earth's lower mantle. Nature 428, 409 (2004).

34. M. B. Duke, Metallic iron in basaltic achondrites. Journal of Geophysical Research 70, 1523 (1965).

35. R. J. Floran et al., Mineralogy, petrology, and trace-element geochemistry of the Johnstown meteorite - a brecciated orthopyroxenite with siderophile and REE-rich components. Geochimica et Cosmochimica Acta 45, 2385 (1981).

36. M. Humayun, A. J. Irving, S. M. Kuehner, Siderophile elements in metal from metal-rich angrite NWA 2999, Lunar Planet. Sci. Conf. XXXVIII, 1221 (2007).

37. R. M. Canup, E. Asphaug, Origin of the Moon in a giant impact near the end of the Earth's formation. Nature 412, 708 (2001).

38. A. J. V. Riches, J. M. D. Day, R. J. Walker, Y. Liu, L. A. Taylor, Highly siderophile-element and osmium isotope constraints on the evolution of angrites, Lunar Planet. Sci. Conf. XLII, 2288 (2011).

39. R. J. Walker et al., Abundances of highly siderophile elements in diogenites compared with the mantle of Earth, Mars and the Moon: Consistent with stochastic late accretion?, Lunar Planet. Sci. Conf. XLII, 1386 (2011).

40. E. Anders, N. Grevesse, Abundances of the Elements - Meteoritic and Solar. Geochimica Et Cosmochimica Acta 53, 197 (1989).

41. M. Wadhwa, in Oxygen in the Solar System, G. J. MacPherson, D. W. Mittlefehldt, J. H. Jones, S. B. Simon, Eds. (2008), vol. 68, pp. 493-510.

42. D. Canil, Vanadium partitioning and the oxidation state of Archaean komatiite magmas. Nature 389, 842 (1997).

43. D. Trail, E. B. Watson, N. D. Tailby, The oxidation state of Hadean magmas and implications for early Earth’s atmosphere. Nature 480, 79 (2011).

44. R. C. Greenwood et al., Has Dawn gone to the wrong asteroid?: Oxygen isotope constraints on the nature and composition of the HED parent body, Lunar Planet. Sci. Conf. XLIII, 2711 (2012).

45. R. J. Walker, M. F. Horan, C. K. Shearer, J. J. Papike, Low abundances of highly siderophile elements in the lunar mantle: evidence for prolonged late accretion. Earth and Planetary Science Letters 224, 399 (2004).

46. A. Yamaguchi et al., Crustal partial melting on Vesta: Evidence from highly metamorphosed eucrites. Geochimica et Cosmochimica Acta 73, 7162 (2009).

47. W. H. Cleverly, E. Jarosewich, B. Mason, Camel Donga Meteorite, a New Eucrite from the Nullarbor Plain, Western Australia. Meteoritics 21, 263 (1986).

48. K. Kaneda, P. H. Warren, M. Miyamoto, Petrology and thermal history of Mg-rich pyroxene bearing cumulate eucrite, Talampaya, Lunar Planet. Sci. Conf. XXXI, 2069 (2000).

49. K. Domanik, S. Kolar, D. Musselwhite, M. J. Drake, Accessory silicate mineral assemblages in the Bilanga diogenite: A petrographic study. Meteorit. Planet. Sci. 39, 567 (2004).

50. J. A. Barrat et al., Geochemistry of diogenites: Still more diversity in their parental melts. Meteorit. Planet. Sci. 43, 1759 (2008).

51. A. Yamaguchi, H. Takeda, J. A. Barrat, Petrology of ferroan diogenites, Yamato 75032 type, Asuka 881839, and Dhofar 700, Lunar Planet. Sci. Conf. XL, 1547 (2009).

52. G. L. Nord, Thermal and Mechanical History of Tatahouine Diogenite. Meteoritics 18, 364 (1983).

53. A. J. Irving et al., Petrology and multi-isotopic composition of olivine diogenite NWA 1877: A mantle peridotite in the proposed HEDO group of meteorites, Lunar Planet. Sci. Conf. XXXVI, 2188 (2005).

54. A. Yamaguchi, T. Setoyanagi, M. Ebihara, An anomalous eucrite, Dhofar 007, and a possible genetic relationship with mesosiderites. Meteorit. Planet. Sci. 41, 863 (2006).

55. H. Y. McSween, What we have learned about Mars from SNC meteorites. Meteoritics 29, 757 (1994).

56. D. W. Mittlefehldt, M. Killgore, M. T. Lee, Petrology and geochemistry of D'Orbigny, geochemistry of Sahara 99555, and the origin of angrites. Meteorit. Planet. Sci. 37, 345 (2002).

57. M. Gellissen, H. Palme, R. L. Korotev, A. J. Irving, NWA 2999, a unique angrite with a large chondritic component, Lunar Planet. Sci. Conf. XXXVIII, 1612 (2007).

58. J. L. Birck, M. R. Barman, F. Capmas, Re-Os isotopic measurements at the femtomole level in natural samples. Geostand. Newsl. 20, 19 (1997).

59. A. S. Cohen, F. G. Waters, Separation of osmium from geological materials by solvent extraction for analysis by thermal ionisation mass spectrometry. Anal. Chim. Acta 332, 269 (1996).

60. D. G. Pearson, S. J. Woodland, Solvent extraction/anion exchange separation and determination of PGEs (Os, Ir, Pt, Pd, Ru) and Re-Os isotopes in geological samples by isotope dilution ICP-MS. Chemical Geology 165, 87 (2000).

61. K. Shinotsuka, K. Suzuki, Simultaneous determination of platinum group elements and rhenium in rock samples using isotope dilution inductively coupled plasma mass spectrometry after cation exchange separation followed by solvent extraction. Anal. Chim. Acta 603, 129 (2007).

62. A. Luguet, G. M. Nowell, D. G. Pearson, 184Os/188Os and 186Os/188Os measurements by Negative Thermal Ionisation Mass Spectrometry (N-TIMS): Effects of interfering element and mass fractionation corrections on data accuracy and precision. Chemical Geology 248, 342 (2008).

63. C. W. Dale et al., Highly siderophile element behaviour accompanying subduction of oceanic crust: Whole rock and mineral-scale insights from a high-pressure terrain. Geochimica et Cosmochimica Acta 73, 1394 (2009).

64. K. R. Ludwig, Calculation of Uncertainties of U-Pb Isotope Data. Earth and Planetary Science Letters 46, 212 (1980).

65. W. F. McDonough, S.-s. Sun, The composition of the Earth. Chemical Geology 120, 223 (1995).

66. P. H. Warren, G. W. Kallemeyn, F. T. Kyte, Origin of planetary cores: Evidence from highly siderophile elements in martian meteorites. Geochimica Et Cosmochimica Acta 63, 2105 (1999).

67. A. D. Brandon, D. W. Graham, T. Waight, B. Gautason, 186Os and 187Os enrichments and high-3He/4He sources in the Earth's mantle: Evidence from Icelandic picrites. Geochimica et Cosmochimica Acta 71, 4570 (2007).

68. P. Momme, N. Oskarsson, R. R. Keays, Platinum-group elements in the Icelandic rift system: melting processes and mantle sources beneath Iceland. Chemical Geology 196, 209 (2003).

69. P. Momme, C. Tegner, C. K. Brooks, R. R. Keays, The behaviour of platinum-group elements in basalts from the East Greenland rifted margin. Contrib. Mineral. Petrol. 143, 133 (2002).

70. I. Puchtel, M. Humayun, Platinum group elements in Kostomuksha komatiites and basalts: Implications for oceanic crust recycling and core-mantle interaction. Geochimica Et Cosmochimica Acta 64, 4227 (2000).

71. I. S. Puchtel, A. D. Brandon, M. Humayun, Precise Pt-Re-Os isotope systematics of the mantle from 2.7-Ga komatiites. Earth and Planetary Science Letters 224, 157 (2004).

72. A. Bezos, J. P. Lorand, E. Humler, M. Gros, Platinum-group element systematics in Mid-Oceanic Ridge basaltic glasses from the Pacific, Atlantic, and Indian Oceans. Geochimica et Cosmochimica Acta 69, 2613 (2005).

73. C. W. Dale, A. Luguet, C. G. Macpherson, D. G. Pearson, R. Hickey-Vargas, Extreme platinum-group element fractionation and variable Os isotope compositions in Philippine Sea Plate basalts: Tracing mantle source heterogeneity. Chemical Geology 248, 213 (2008).

74. M. Rehkämper et al., Ir, Ru, Pt, and Pd in basalts and komatiites: New constraints for the geochemical behavior of the platinum-group elements in the mantle. Geochimica et Cosmochimica Acta 63, 3915 (1999).

75. M. F. Horan, R. J. Walker, J. W. Morgan, J. N. Grossman, A. E. Rubin, Highly siderophile elements in chondrites. Chemical Geology 196, 5 (2003).

76. R. J. Walker et al., Comparative Re-187-Os-187 systematics of chondrites: Implications regarding early solar system processes. Geochimica et Cosmochimica Acta 66, 4187 (2002).

77. K. Righter, M. J. Drake, A magma ocean on Vesta: Core formation and petrogenesis of eucrites and diogenites. Meteorit. Planet. Sci. 32, 929 (1997).

78. P. H. Warren, G. W. Kallemeyn, H. Huber, F. Ulff-Moller, W. Choe, Siderophile and other geochemical constraints on mixing relationships among HED-meteoritic breccias. Geochimica et Cosmochimica Acta 73, 5918 (2009).

79. A. Borisov, H. Palme, Experimental determination of the solubility of platinum in silicate melts. Geochimica et Cosmochimica Acta 61, 4349 (1997).

80. E. Cottrell, D. Walker, Constraints on core formation from Pt partitioning in mafic silicate liquids at high temperatures. Geochimica et Cosmochimica Acta 70, 1565 (2006).

81. E. Ohtani, H. Yurimoto, Element partitioning between metallic liquid, magnesiowustite, and silicate liquid at 20 GPa and 2500 degrees C: A secondary ion mass spectrometric study. Geophys. Res. Lett. 23, 1993 (1996).

82. W. Ertel, H. S. C. O'Neill, P. J. Sylvester, D. B. Dingwell, B. Spettel, The solubility of rhenium in silicate melts: Implications for the geochemical properties of rhenium at high temperatures. Geochimica et Cosmochimica Acta 65, 2161 (2001).

83. S. S. Fortenfant, D. Gunther, D. B. Dingwell, D. C. Rubie, Temperature dependence of Pt and Rh solubilities in a haplobasaltic melt. Geochimica et Cosmochimica Acta 67, 123 (2003).

84. S. S. Fortenfant et al., Oxygen fugacity dependence of Os solubility in haplobasaltic melt. Geochimica et Cosmochimica Acta 70, 742 (2006).

85. K. Righter, M. J. Drake, Metal-silicate equilibrium in a homogeneously accreting earth: New results for Re. Earth and Planetary Science Letters 146, 541 (1997).

We are grateful to the Natural History Museum for provision of numerous samples. C.D. acknowledges funding from grant NER/C51902X/1 from the Natural Environment Research Council, UK. We thank three anonymous referees and the editor, M. Cruz, for their constructive comments. We also thank H. Williams for useful discussions. Full HSE and Os isotope data are available in Supporting Online Material (www.sciencemag.org): Materials and Methods, Supporting Online Text, Table S1, Figs. S1-S4, References (44-84).

Table 1. Average sample HSE concentrations and estimated mantle HSE concentrations for each parent body.

	Os ng/g	Ir ng/g	Ru ng/g	Pt ng/g	Pd ng/g	Re ng/g	**Total** ng/g
Earth (ref. 3)	3.92	3.50	7.11	7.74	7.21	0.32	**29.8**
Vesta (HED parent body)							
Average diogenites	0.020	0.014	0.046	0.15	0.12	0.006	
Average eucrites	0.025	0.022	0.038	0.10	0.21	0.006	
Mantle estimate	0.07	0.07	0.10	0.12	0.04	0.004	**0.40**
High	0.18	0.18	0.25	0.35	0.10	0.016	
Low	0.03	0.03	0.04	0.03	0.01	0.001	
Angrite PB							
Average	0.50	0.60	0.83	2.0	1.1	0.91	
Mantle estimate	1.5	1.5	2	3	1.8	0.1	**10**
Pasamonte PB (n=1)							
Average	0.424	0.629	1.33	1.69	1.29	0.054	
Mantle estimate	1	1	1.5	2	1.2	0.08	**7**
Ibitira PB (n=1)							
Average	0.018	0.019	0.029	-	0.018	<0.001	
Mantle estimate	0.01	0.01	0.01	0.02	0.02	0.002	**7**
Mars[a]							
Average	0.96	0.98	1.8	8.4	10.0	0.12	
Mantle estimate	2.4	2.4	3	4	3	0.1	**15**
High	3.5	3.5.	4	5	4	0.2	
Low	1.5	1.5	1.5	2.5	1.5	0.05	
Moon[b]							
Mantle estimate	0.07	0.07	0.10	0.10	0.03	0.004	**0.37**
High	0.13	0.13	0.15	0.15	0.04	0.005	
Low	0.04	0.04	0.05	0.03	0.01	0.001	
Moon - Estimate from ref. 12	0.1	0.1	0.1	0.2	0.1	0.01	0.6

NOTES: All mantle concentrations estimated by incompatible/compatible HSE ratio method (*21*), except published estimate for the lunar mantle which was derived from regression of MgO vs. HSE. Estimated uncertainties are included except where the small number of samples analysed makes such estimation impossible. Estimate for Vesta based on 'undisturbed' samples (*21*). Estimates for Pasamonte and Ibitira based on inferred chondritic proportions and similar slopes in ratio plots to other parent body melts. [a] Mars average and mantle estimate includes data from (*5*), [b] Moon estimate used 'undisturbed' data from (*15, 16*).

Figure captions

Fig. 1. **(A)** Mean HSE concentrations for each achondrite group, normalised to CI chondrite; **(B)** Mantle HSE concentrations in each parent body estimated using the HSE ratio method (Fig. 2; *21*); **(Inset)** HSE concentrations in Earth's mantle compared with calculated mantle abundances remaining after low-pressure (applicable to Vesta) and high-pressure equilibrium metal-silicate partitioning during core formation [upper bound of high-pressure partitioning is displayed, but a greater discrepancy between calculated and observed concentrations for some elements is likely (*21*)]. Relative HSE proportions in the silicate mantles of the various parent bodies are all broadly chondritic, but the absolute concentrations vary by 2 orders of magnitude. Lunar mantle melts (*15*) shown for comparison in A; CI chondrite values from (*40*). Earth's mantle from (*3*). For lunar and martian mantle estimates see Table 1 notes.

Fig. 2. Estimation of parent body mantle HSE abundances using incompatible/compatible HSE ratios (*21*). Platinum is more incompatible than Os during mantle melting. High melt fractions have low Pt/Os ratios and high Os that approach the HSE content of the source mantle. Large symbols for HED indicate the least 'disturbed' samples in terms of having broadly chondritic initial Os isotope compositions and smooth HSE patterns (*21*), faint HED field encompasses all samples. For data sources see Fig S2.

Fig. 3. Total HSE concentration estimated for each parent body mantle relative to **(A)** parent body mass; **(B)** oxidation state (defined in log units relative to the iron-wüstite buffer) (*41*). While the oxidation state for the Earth (present-day upper mantle) and Mars do not necessary reflect conditions at the time of late accretion, there is strong evidence for pre-4 Gyr establishment of present-day levels of oxidation (*42, 43*), and an increase in oxygen fugacity during core formation is required to account for moderately siderophile element abundances in the Earth's mantle (*32*). A linear relationship in (B) provides a good fit, but a non-linear relationship is also plausible, with low mantle HSE contents below the IW buffer and a rapid increase in oxidation of late-accreted metal, and hence mantle HSE concentration, once a threshold oxygen fugacity is exceeded. For lunar and martian mantle HSE concentration estimates see Table 1 notes. Uncertainty for angrite PB assumed to be the same as for Mars.

#

Figure 1

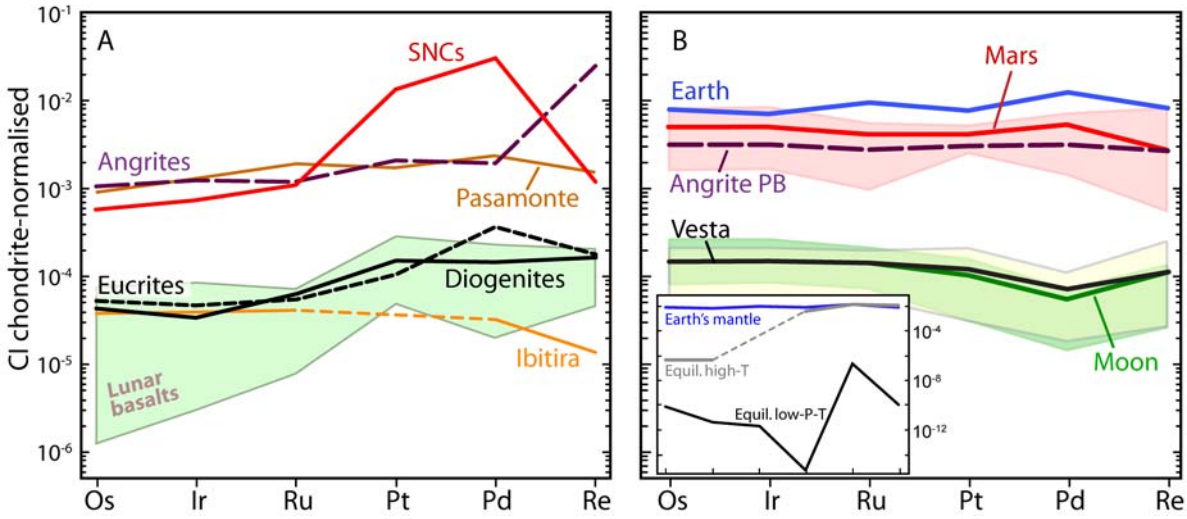

Figure 2

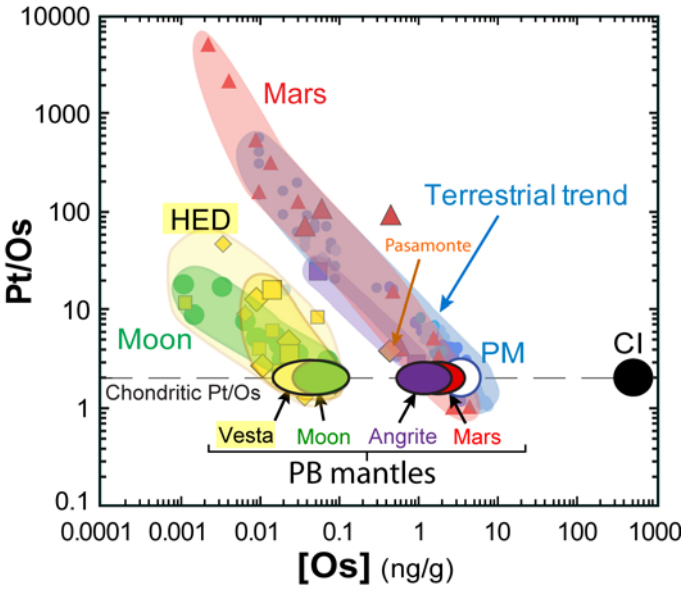

Figure 3

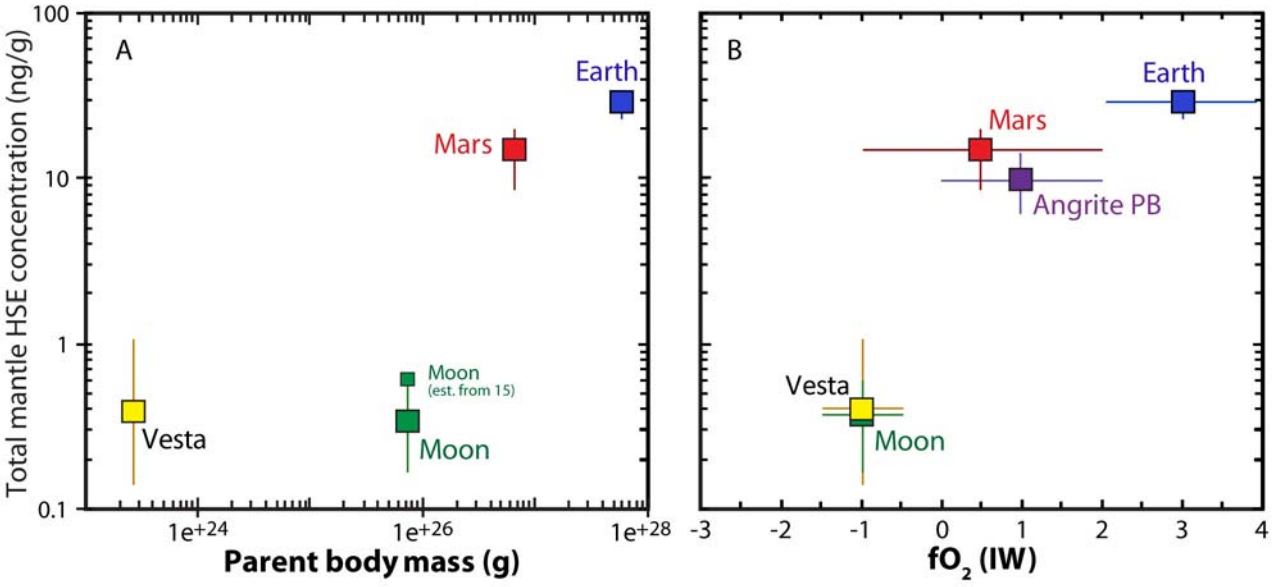
A
Earth
Mars
Moon
(est. from 15)
Moon
Vesta
Total mantle HSE concentration (ng/g)
100
10
1
0.1
1e+24
1e+26
1e+28
Parent body mass (g)
B
Earth
Mars
Angrite PB
Vesta
Moon
-3
-2
-1
0
1
2
3
4
fO2 (IW)

Supplementary Online Material

SOM – Materials and methods

Samples chosen were mostly 'falls' rather than 'finds' (see sample details below), i.e. meteorites which had been observed falling to Earth rather than found without knowledge of the length of time on Earth. This limits the possible effects of terrestrial alteration and weathering. Oxygen isotope data confirm that significant terrestrial alteration has not occurred (see 'notes on samples' below). While all HEDs display a degree of brecciation, there is no oxygen isotope evidence for meteoritic contamination except in the case of Dhofar 007, which has a non-HED oxygen isotope composition (*44*). This precludes significant contamination by differentiated HSE-poor material, but does not altogether preclude HSE contamination by chondritic or metal-rich impactors which have much higher HSE concentrations, and therefore much smaller contributions are required to affect HSE contents. However, if any samples in this study contained significant HSE from such impactors, the resulting HSE patterns would be chondritic and would not display the platinum-group PGE/iridium-group PGE fractionation found in most samples. Johnstown, NWA2999 and Dhofar007 are exceptions which all have unfractionated HSE patterns and are all known to have high metal contents, and contain Ni-rich metal, indicating direct addition of impactor material after crystallisation. These three samples have been omitted from estimates and discussion. In the unlikely event that other HEDs did contain an HSE-rich contaminant, this would merely further strengthen our findings that the HED parent body has very low HSE contents. If any form of alteration and contamination has occurred, it is difficult to reconcile this with the array formed by samples in HSE ratios plots (e.g. Fig S3 and see below)

Nevertheless, some samples do have Re and Os concentrations that are not consistent with a chondritic initial Os isotope composition, even accounting for the not inconsiderable effect of analytical uncertainty on low-level measurements which are then time-integrated over approximately 4500 Myrs (e.g. gamma Os values that are more than 100 units from chondrite). In these cases, samples have been omitted from estimates, although the data are still plotted on figures. Furthermore, as this effect is likely due to Re mobility (e.g. *45*), emphasis has instead been placed on HSE ratio plots that do not involve Re, for example Pt/Os, which should be more robust both analytically (higher Pt concentrations than Re by 5-500 times) and geologically, as Pt is less susceptible to alteration and mobilisation.

Notes on Samples

Agoult (Find 2000), very fresh, unbrecciated, granulitic-textured eucrite. Shows no geochemical evidence of weathering, such as high Ba and Sr abundances, positive Ce anomalies or perturbed Th/U ratios (*46*). Oxygen isotope analysis of Agoult gave a mean $\Delta^{17}O$ value of -0.239 ± 0.034 ‰(2σ) (*46*), which is identical to the average HED $\Delta^{17}O$ value of -0.239‰ ± 0.014 (2σ) (*19*). This result is consistent with the evidence that Agoult is both un-weathered, and uncontaminated by meteoritic material.

Bereba (Fall 1924), monomict eucrite. As a monomict eucrite, Bereba is unlikely to contain any significant amount of meteoritic contamination. Mean $\Delta^{17}O$ value of -0.240 ± 0.044 ‰(2σ) (*19*), which is indistinguishable from the HED average (*19*). This result is consistent with Bereba being pristine with respect to terrestrial contamination (i.e. a fall), with no evidence of meteoritic contamination.

Camel Donga (Find 1984), fresh monomict eucrite, with most specimens covered in primary black fusion crust (*47*). Camel Donga shows no evidence of either terrestrial or meteoritic contamination.

Juvinas (Fall 1821), monomict eucrite. Mean $\Delta^{17}O$ value of -0.230‰ ± 0.012 (2σ) (*19*), within error of the HED average (*19*). In keeping with its monomict character, this result indicates that Juvinas is free of any meteoritic contamination.

Millbillillie (Fall 1960), monomict eucrite. Mean $\Delta^{17}O$ value of -0.246‰ ± 0.036 (2σ) (*19*), within error of the HED average (*19*). This result, and its monomict character, precludes significant contamination by meteoritic material.

Stannern (Fall 1808), monomict eucrite. Mean $\Delta^{17}O$ value of -0.245‰ ± 0.018 (2σ) (*19*), which is within error of the HED average (*19*). Given its monomict character, this result suggests that Stannern is uncontaminated by meteoritic material.

Talampaya (Fall 1995), brecciated cumulate eucrite (*48*). Although this sample is both brecciated and metamorphosed, there is no evidence that it has been contaminated by non-HED meteoritic material.

Bilanga (Fall 1999), diogenite. Extensively brecciated and contains a range of different lithologies (*49*). Mean $\Delta^{17}O$ value of -0.239‰ ± 0.044 (2σ) (*19*), in agreement with the HED average (*19*). Despite the brecciated nature of this sample, there is no evidence to suggest that it has been significantly contaminated by non-HED meteoritic material (*50*).

Dhofar 700 (Find 2002), unbrecciated diogenite with a granular texture (*50, 51*). Slightly weathered and displays some fractures filled with secondary carbonates and Fe-hydroxides (*50*). A mean $\Delta^{17}O$ value of -0.25‰ ± 0.02 (2σ) was obtained on an EATG-washed fraction of Dhofar 700 (*50*), within error of the HED average (*19*). This result indicates that Dhofar 700 is free of significant meteoritic contamination.

Johnstown (Fall 1924), brecciated diogenite containing centimetre-sized clasts (*35, 50*). Displays a wide range of Ni and Co abundances (Ni = 37–460 μg/g, Co = 12–85 μg/g) (*50*). This large range in values has been interpreted, although disputed (*50*), as being due to an externally-derived meteoritic component (*35*).

Shalka (Fall 1850), diogenite. Mean $\Delta^{17}O$ value of -0.242‰ ± 0.032 (2σ) (*19*), within error of the mean for the HED group (*19*). There is no evidence that Shalka has experienced either terrestrial or meteoritic contamination.

Tatahouine (Fall 1931), diogenite. A unique diogenite in that it fell as single orthopyroxene crystals, other diogenites being essentially fragmental breccias (*52*). Mean $\Delta^{17}O$ value of -0.239‰ ± 0.030 (2σ) (*19*), within error of HED mean (*19*). There is no evidence that Tatahouine has experienced either terrestrial or meteoritic contamination.

NWA 1877 (Find 2003), olivine-rich diogenite. Coarse-grained rock with an olivine content of approximately 45% and shows only minor evidence of terrestrial contamination (*53*). Oxygen isotope analysis of acid washed mafic silicates gave $\Delta^{17}O$ values (*53*) close to HED average values (*19*). NWA 1877 shows no evidence for meteoritic contamination.

NWA 2629 (Find 2004), olivine-rich diogenite. Probably paired with NWA 1877.

Ibitira (Fall 1957), monomict eucrite. Along with NWA 011, a wide range of geochemical evidence now exists to indicate that Ibitira is from a distinct parent body to that of the HEDs (21). There is no evidence that Ibitira has been contaminated by meteoritic material.

Pasamonte (Fall 1933), polymict eucrite. Considered to be from a distinct parent body to the other HEDs (*22*). An alternative possibility that it is a normal HED with approximately 3% contamination by an ordinary chondrite impactor (*19*) was rejected on the basis that Ni and Ir in Pasamonte are far too low to be explained by such a scenario (*22*).

Dhofar 007 (Find 1999), cumulate eucrite. Complex polymict breccia, with possible affinities to the mesosiderites (*54*). Dhofar 007 has an oxygen isotope composition that plots outside the normal HED range (*19*). Dhofar 007 has a highly elevated siderophile content, with one clast containing 929 ppm Ni (*54*). Thus,

Dhofar 007 shows clear evidence of having experienced significant meteoritic contamination. It shows only minor evidence of terrestrial contamination.

Chassigny (Fall 1815), Martian chassignite. One of only two currently identified chassignites (the other being NWA 2737). Dunite consisting predominantly of Fe-rich olivine, with various minor phases including pigeonite, augite, alkali feldspar, chromite, ilmenite and rutile (*55*).

Nakhla (Fall 1911), Martian nakhlite. The type nakhlite, Nakhla consists predominantly of magnesian augite with subordinate Fe-rich olivine, set in a microcrystalline matrix (*55*).

Shergotty (Fall 1865) and Zagami (Fall 1962), Martian basaltic shergottites. Both relatively fine-grained rocks, consisting predominantly of augite and pigeonite, with subordinate maskelynite, titanomagnetite, ilmenite, whitlockite and accessory apatite, quartz, fayalite and mesostasis (*55*).

D'Orbigny (Find 1979), angrite. Vesicular, unshocked and unmetamorphosed igneous lithology composed of Al-Ti-rich clinopyroxene, Ca-rich olivine, kirschsteinite, anorthite and a range of accessory phases (*56*).

NWA 2999 (Find 2004), angrite. Coarse-grained, polygonal-granular texture similar to that seen in the angrites Angra dos Ries and LEW 86010. Compared to other angrites, NWA 2999 shows very high Ni and Co concentrations, which have been interpreted as indicating that the meteorite contains a high chondritic component (*57*).

Sahara 99555 (Find 1999), angrite. Vesiculated, igneous-textured lithology, which shows many similarities to D'Orbigny in terms of its chemical composition and mineralogy (*56*).

Methods

Digestion and purification. Samples were all hand-crushed and ground in an agate pestle and mortar. Powders (see Table S1 for weights) were placed in quartz high-pressure asher (HPA) vessels together with a mixed ^{190}Os-^{185}Re-^{99}Ru-^{106}Pd-^{191}Ir-^{194}Pt-enriched spike and inverse aqua regia: 1 - 2.5 mL 12 mol L^{-1} HCl, 2 - 5 mL 16 mol L^{-1} HNO_3 (quantity depending on sample mass). The vessels were placed in an Anton Paar HPA at 300°C for at least 12 hours, in order to extract the HSE and achieve full sample-spike equilibration. Osmium was extracted using CCl_4, back-extracted into 9 mol l^{-1} HBr, and then microdistilled (*58, 59*). The inverse aqua regia was dried and prepared for purification of Re, Ir, Pt, Ru and Pd using AG1X-8 (100-200#) anion-exchange resin (*60*). Due to the isobaric interference of ZrO^+ on Pd^+, the solvent N-benzoyl-N-phenyl-hydroxylamine was mixed with and extracted from the final sample solutions in order to extract any remaining Zr after column separation (*61*). A further modification to the previous protocol was the addition of H_2O_2 during preparation for anion-exchange separation in order to reduce any Cr^{6+} formed during digestion. This step leads to more efficient Cr elution prior to HSE collection during chromatographic separation, and consequently reduces potential isobaric interferences of multi-oxide Cr species with Ru isotopes during mass spectrometry.

Mass spectrometry. Os was loaded onto Pt filaments and measured as OsO_3^- ions by negative-thermal ionisation mass spectrometry (N-TIMS) using the ThermoFinnigan Triton at Durham University. Raw data were corrected offline for O isotope interference, mass fractionation (using ^{192}Os/^{188}Os = 3.08271) and spike unmixing. Interference from $^{187}ReO_3^-$ was insignificant (≤2 cps). Analyses of 1 and 10 pg aliquots of the Durham Romil Os standard solution (DROsS) gave a mean ^{187}Os/^{188}Os of 0.16106 ± 0.00138 (~0.8% 2 RSD, n=19) for the period of analysis, December 2008 - January 2011. These values are in good agreement with a value of 0.160924 ± 4 for 10-100 ng/g aliquots measured on the same mass spectrometer in Faraday cup mode (*62*). Rhenium, Ir, Ru, Pt, Pd were analysed by inductively-coupled plasma mass spectrometry (ICP-MS) on a ThermoFinnigan® Element 2. Standard HSE, Hf, Zr, Y and Mo solutions (all 1 ppb) were analysed at the start, middle and end of each session to quantify the degree of mass fractionation and the production rates of HfO^+,

ZrO^+, YO^+ and MoO^+ (<0.6, <1.5, <0.8, <0.2%, respectively) which have equivalent masses to isotopes of Ir^+, Pt^+ and Pd^+.

Blanks. Average blanks (n=4) were as follows (with 2sd in parentheses): 0.1 pg Os (0.07), 0.35 pg Ir (0.4), 2.5 pg Ru (3.1), 5.6 pg Pt (4.4), 7.1 pg Pd (17.5), 1.4 pg Re (1.3), with a mean $^{187}Os/^{188}Os$ of 0.21 ± 0.07. These quoted uncertainties are probably overestimated because they include blanks measured in different analytical sessions with different reagent batches. For this reason, blank correction was made using blanks for each analytical period. With the exception of one very HSE-poor olivine diogenite, the contribution of the blank to the analysis was <5% for Os, and typically <8% for Ir (max 32%), <23% for Ru (32%), <16% for Pt (23%), <30% for Pd (75%) and <40% for Re (65%). The difference between measured and corrected $^{187}Os/^{188}Os$ was never greater than 10%.

Reproducibility. The uncertainties on individual measurements are typically low (<5%), but the overall uncertainty for the concentration of HSE in a given sample (i.e. duplicate analyses of aliquots of the same powder) is significantly higher and, due to the limited amount of available sample, is not precisely constrained in this study. Duplicate analyses (n=7 x 1 g) of a CANMET basaltic reference material, TDB-1, indicates reproducibility of 7% for Re concentration, 17-25% for Os, Ir, Pt and Pd and 34% for Ru - which is thought largely to be due to heterogeneity within the powder rather than analytical uncertainty as concentrations and elemental ratios are significantly more reproducible for some other samples with similar HSE abundances, for instance 4-12% for all HSE ratios (n=3) in a terrestrial gabbro (*63*). Duplicate analyses of two achondrites indicate variable reproducibility (at sub-1g powder mass), depending on the sample and the element in question, but all standard deviations are less than 60%, e.g. Os, Ir and Re are reproducible for the diogenite Tatahouine (standard deviation within 25%), while Pt is less so (s.d. ~50%, see Table S1 and Fig. S1). Regardless of the absolute reproducibility for the achondrites, duplicate analyses confirm chondritic proportions of HSE in the melt source and give consistent estimates of mantle source HSE abundance when using the incompatible/compatible HSE ratio method below.

Supporting Online Text – Estimation of parent body mantle HSE abundances

Using MgO vs [HSE]

Previous work (e.g. *15*) has utilised the positive co-variation of MgO and HSE concentrations in terrestrial samples to extrapolate from relatively MgO-poor crustal samples (e.g. 8 wt% MgO) towards the MgO content of typical mantle (~35 wt%). The central tenet of this method is that the HSE behave similarly during melting of different planetary mantles as they do on Earth. Given known differences in pressure and temperature of melting, and good evidence for differing oxygen fugacity, sulphur contents, mineralogy and bulk composition in the mantles of the various parental bodies (PBs), it seems unlikely that this assumption of similar behaviour is robust. Eucrites and diogenites, both thought to be from the asteroid 4-Vesta, have similar HSE contents despite very different MgO (~8 wt% and ~20-30 wt%, respectively, Fig. S3). This results in disparate estimates for mantle concentrations from the two suites if taken individually. In addition, too few data and/or data with little spread in MgO preclude estimation of some PB mantle abundances. For these reasons we instead use the method below to estimate mantle HSE abundances.

Using [HSE_a] vs HSE_b/HSE_a plots (e.g. [Os] vs Pt/Os)

An alternative method for the estimation of mantle abundances is by comparison of concentrations of two HSE of differing compatibility. At low degrees of melting incompatible/compatible HSE ratios will be high, and as melting degree increases such ratios will decrease, until at high melting degrees the ratio will be approximately equal to the source. This gives a negative co-variation between the ratio and the concentration of the denominator (Fig S4a-b); e.g. Re is moderately incompatible, Os is compatible, so low-degree melting produces

high Re/Os and low Os concentrations, whereas high-degree melting produces low Re/Os and high Os concentrations. This method is independent of partitioning behaviour; any difference in HSE compatibility (compared to Earth), due to differing source mineralogy and melting conditions, may alter the slope of a trend but the same origin will be retained. This should also hold for cumulate rocks, such as some of the HEDs studied here, where partitioning may differ from that in a melt, but the array origin will remain the same. This is illustrated by terrestrial cumulate gabbros (*63*), which define a lesser slope but with the same primitive mantle origin. It is possible, however, that a cumulate rock may fall on an array which derives from a point on the mantle melt array (the main trend) but diverges from this trend due to different elemental partitioning in an isolated melt system. Accumulation of a greater proportion of a certain mineral may also affect the partitioning behaviour and lead to the sample plotting off the main trend. The cumulate nature of some HED samples, particularly the diogenites, may thus contribute to the scatter of the data, and give rise to a greater uncertainty on the Vestan mantle estimate. But the presence of a trend with a termination at chondritic Pt/Os (for example) suggests this effect is relatively minor, and that this method of estimation is valid. Once the criterion of non-disturbance is implemented (i.e. 'disturbed' samples are omitted), five of the seven diogenites are discarded from the estimate, whereas four of the seven eucrites are retained, none of which are cumulates. This means that the estimate is weighted towards non-cumulate samples, and the greater scatter of diogenites (Fig. S3) is largely circumvented in the estimate. In order to fully assess our uncertainties, we have calculated error envelopes for the Pt/Os and Re/Os data using the method of Ludwig (*64*). The entire range of possible HSE concentrations for Vesta is between 20 and 100 times lower than the Earth's mantle.

In sample suites with a range of MgO (and therefore HSE contents) approaching the composition of mantle, the mantle HSE concentration can be estimated to be the terminus of the trend at the highest concentration. However, as discussed for the MgO-HSE method above, some suites do not possess such a range of MgO contents. In these cases, the mantle concentration can be estimated by extension of the trend towards higher concentrations (of the denominator), to the point where the incompatible/compatible HSE ratio is equal to that found in chondrites. In these cases, the method assumes chondritic proportions of the HSE – while this is somewhat circular, it is supported by the measured HSE concentrations in almost all achondrites. Measured concentrations do not show significant fractionation of HSE from chondritic proportions, except the relatively minor Pt, Pd and Re enrichment which reflects differing compatibility during partial mantle melting (Fig. S1). Broadly chondritic Os isotopes are also consistent with this assumption (Figs. S4). In addition, although there is a degree of uncertainty as to whether the true origin of each array is well-represented by the data available (i.e. it could fall at lower Re/Os or Pt/Os and higher Os concentration) it is notable that there are very few achondrite samples measured which fall below the chondrite reference line. This again confirms that parent body HSE proportions are approximately chondritic. For the anomalous eucrites (Ibitira and Pasamonte), there is only one sample for each parent body. Thus, estimates of mantle abundances are largely unconstrained and rely on the assumption of chondritic proportions and a slope similar to that for the Earth. The estimates for the anomalous eucrites have been included in Table 1 but not plotted in Figs. 1b or 3.

Given that there is considerable variation on incompatible/compatible HSE plots within most achondrite suites, perhaps reflecting incomplete mixing of the PB mantle, estimates of mantle abundances in this way (as with the other method) carry considerable uncertainties. However, the differences between estimated mantle abundances of the various parent bodies span orders of magnitude compared with uncertainties which are less than a factor of six, even for the scattered Pt/Os data for the HED suite.

Comparison of parent body mantle HSE estimates using the two methods

Estimates of mantle HSE concentrations for Vesta cannot be reliably made using MgO-HSE co-variations because the eucrites and diogenites have similar HSE contents despite very different MgO (~8 wt % and ~20-30 wt%, respectively, Fig. S3). This would result in disparate estimates for mantle concentrations from the two

suites if taken in isolation. By accepting the assumption that concentrations in the MgO-rich diogenites approach those of the Vesta mantle, one could estimate Ir and Os abundances to be of the order of 0.03 ng/g. This compares to a far more robust estimate of 0.07 ng/g Os derived from the array in incompatible/compatible HSE plots. Either way, the estimate is up to two orders of magnitude lower than abundances in Earth's mantle (~3.5 ng/g Os (*3, 65*)).

The concentrations of Os and Ir in the lunar mantle have been estimated previously, using the MgO-HSE method, to be ~0.1 ng/g (*15*)(Fig S2). Applying the HSE ratio method to the same data we estimate concentrations which are slightly lower, but within uncertainty of this value: Ir and Os of ~0.07 ng/g in the lunar mantle. Using MgO-HSE systematics, the Martian samples in this study, with one exception (Shergotty), are in broad agreement with previous estimates that HSE contents of the Martian mantle are only slightly lower than Earth (Os and Ir: ~2.5 ng/g (e.g. *5, 66*)). This value is consistent with the HSE ratio method, illustrating that in some cases the two methods agree. However, by using the MgO-HSE method, anomalously low HSE concentrations in ALH84001 (*66*) would suggest a source more than an order of magnitude poorer in HSE than the other SNCs, whereas the HSE ratio method indicates that the source possibly had lower HSE concentrations, but within a factor of two of the other SNCs. This confirms that conditions and mineralogy during melting are key processes which preclude the use of MgO-HSE systematics in estimating parent body mantle abundances. Only two samples can be used for the angrite estimate, as the third angrite analysed is known to contain a high proportion of impactor metal, which accounts for its extremely high abundances of HSE (≈chondrite). However, both angrites are consistent with a source containing somewhat lower HSE concentrations (~1.5 ng/g Os) than Mars. As the angrites possess a very large range of HSE concentrations over a very limited range of MgO contents, no estimation of mantle abundance is possible using MgO vs HSE.

SOM – Calculation of mantle HSE concentrations after equilibrium metal-silicate partitioning and calculation of fraction of late veneer addition

Depletion factors for the silicate mantle were calculated using the following equation:

$$\text{Depletion factor} = 1/(D_{met/sil} \times F_{core} + F_{silicate})$$

Where D is the distribution coefficient of an element between liquid metal and silicate melt and F_{core} and $F_{silicate}$ are the fractions of core and silicate mantle, respectively, assumed in all cases to be 70% silicate - broadly equivalent to the mass ratio of metal and silicate in the Earth. Depletion factors were calculated for both low- and high-pressure metal-silicate equilibration (for D values see Table S2), and the model silicate mantle concentrations of HSE were then calculated by multiplying the depletion factor by an average chondrite concentration (*12*). High-pressure equilibration was assumed for Earth, both a high- and low-pressure model was used for Mars, and the angrites (unknown parent body size), though the difference is insignificant. Vesta must have formed by low-pressure equilibration. A low pressure model was also used for the Moon, although its formation may be complex given its creation from a giant impact on Earth. Chondritic material was then mixed with the depleted silicate mantles after core formation, until HSE concentrations best matched the estimated values in Fig. 1. Assessment of best fit was achieved by the lowest sum of the deviations between calculated and estimated values for each element (average deviation for Os, Ir, Pt and Pd was between 0.1 and 0.2, Ru and Re were not included due to a lack of a high-pressure partition coefficient for the former and the extremely low concentrations of Re).

Supplementary figures

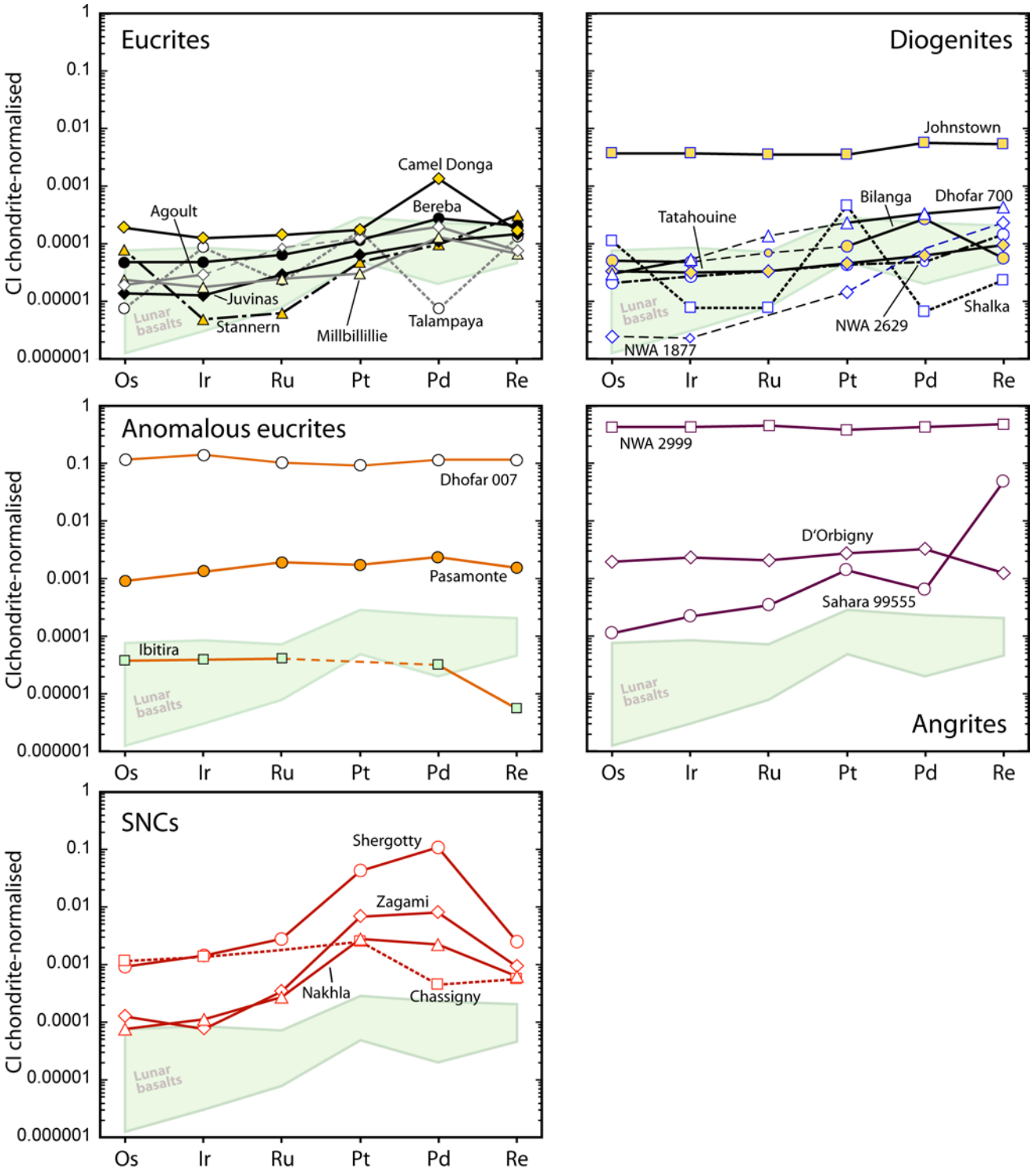

Figure S1. Measured HSE concentrations for all achondrites normalised to CI chondrite. Lunar mantle melt fields are shown for comparison (*15*). Eucrites and diogenites are thought to be from Vesta; anomalous eucrites – unknown parent bodies (PB); angrites – unknown PB; SNCs – Mars. Area above dashed line in the MORB field is the typical range, whole shaded area is complete range. Johnstown, NWA2999 and Dhofar007 are all known to have high metal contents, and Ni-rich metal, indicating direct addition of impactor material after crystallisation. Thus, they are not thought to reflect their mantle source abundances and have been omitted from calculations and discussions in this paper.

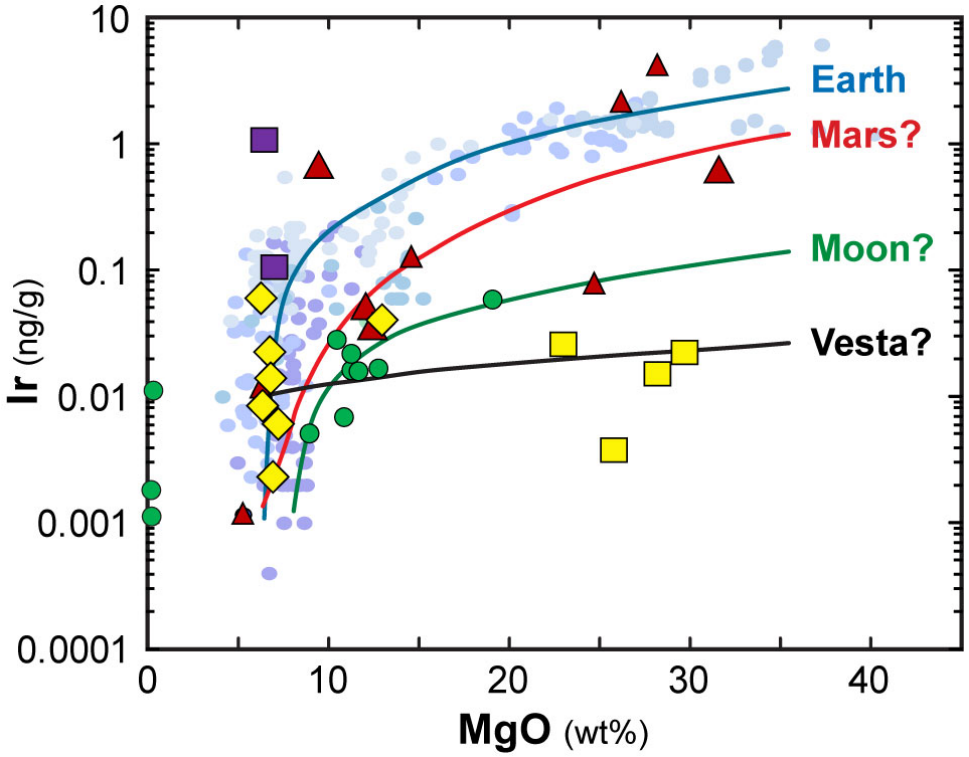

Figure S2. Estimation of parent body mantle HSE abundances by applying the co-variation of MgO and HSEs in terrestrial mantle-derived melts (*15*) to other planetary bodies, and extrapolating to ~35 wt% MgO. Estimates are not possible for Vesta or the angrite parent body due to similar HSE concentrations at differing MgO in the former and a lack of MgO variation in the latter. Other estimates for the Moon and Mars also require significant extrapolation. The incompatible/compatible HSE ratio method is instead preferred and used here. References for terrestrial samples: (*67-74*). Johnstown, NWA2999 and Dhofar 007 omitted due to evidence for post-crystallisation meteoritic contamination (*25*).

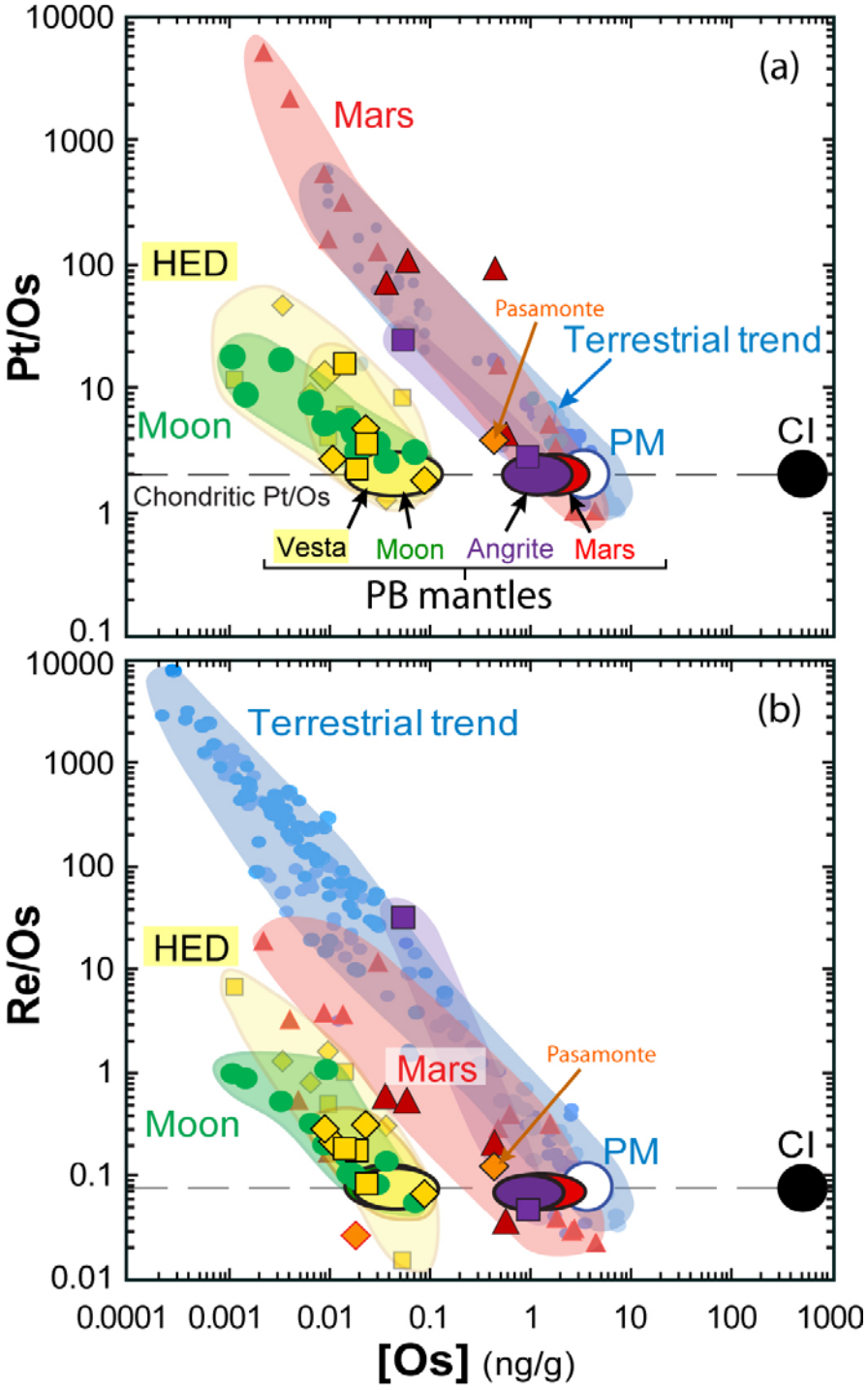

Figure S3. Estimation of parent body mantle HSE abundances using incompatible/compatible HSE ratios. Platinum is more incompatible than Os during mantle melting, thus high Pt/Os ratios are produced by low melt fractions, while the Os concentration is low. At high melt fractions the Pt/Os ratios and Os concentrations are similar to those of the source and thus reflect the HSE content of the source mantle. Any difference in HSE compatibility (compared to Earth), due to differing source mineralogy, pressure, temperature or oxygen fugacity, will only change the slope of the array, while still retaining the same origin. This is in contrast to the HSE vs. MgO method in Fig S2 which may be dependent on these factors. Johnstown, NWA2999 and Dhofar007 omitted due to evidence for post-crystallisation meteoritic contamination (*25*). Only 'undisturbed' lunar and HED samples used for estimation (latter shown as larger yellow symbols). For HED, samples were omitted if they have initial Os isotope compositions more than 90 gamma Os units from chondrite and if their HSE patterns are not smooth. For lunar samples see (*15, 16*), Mars literature data from (*5*). References for terrestrial samples: (*67-74*).

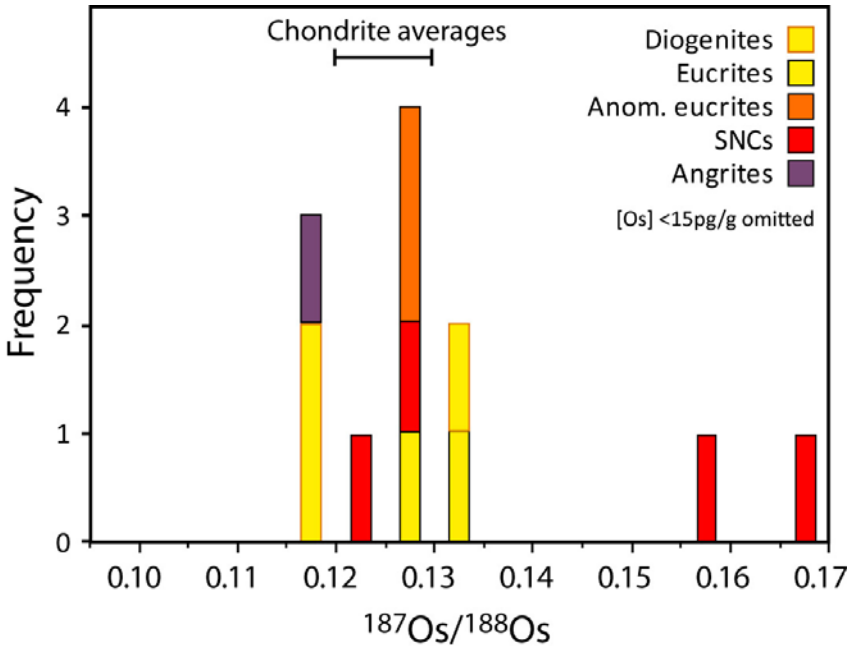

Figure S4. Histogram of measured Os isotopes of individual samples indicating broadly chondritic evolution. Initial ratios are not plotted due to the difficulties in age-correcting for ^{187}Os ingrowth in Re- and Os-poor samples over time periods of up to 4.5 Ga for some samples. Chondrite averages from (*75*).

Table S1. HSE concentrations and Os isotopes in achondrite meteorites: Eucrites, diogenites and olivine diogenites (proposed parent body: 4-Vesta), anomalous eucrites (unknown PBs), SNCs (Mars), angrites (unknown PB).

	Sample mass	MgO wt.%	Os ng/g	Ir ng/g	Ru ng/g	Pt ng/g	Pd ng/g	Re ng/g	Re* ng/g	$^{187}Os/^{188}Os$	$^{187}Re/^{188}Os$	$^{187}Os/^{188}Os$ initial*
Eucrites												
Agoult	0.3226	6.8	0.009 (1)	0.014 (2)	~0.07	0.121(23)	0.112(24)	0.003 (1)	0.001	0.13369 (26)	1.39	-
Bereba	0.7997	6.8	0.024(1)	0.023(2)	0.046(19)	0.113(7)	0.154(17)	0.007(2)	0.002	0.12702 (21)	1.52	0.010
dupl.	0.5758	-	0.010(0)	0.017(1)	-	0.156(12)	-	0.016(2)	0.001	0.13187 (32)	7.81	-
C. Donga	0.5873	6.3	0.090(2)	0.061(4)	0.101(6)	0.168(10)	0.743(26)	0.006(1)	0.009	0.13118 (63)	0.327	0.106
Juvinas BM	0.5092	7.3	0.007(1)	0.006(1)	0.021(3)	0.062(5)	0.061(11)	0.005(2)	<0.001	0.12358 (17)	3.84	-
Millbillillie	0.8896	7.4	0.011(0)	0.009(1)	0.018(2)	0.030(4)	0.072(9)	0.002(0)	0.002	0.15412 (41)	1.05	-
Stannern	0.2788	7.0	0.038(1)	0.002(1)	0.004(4)	0.048(7)	0.054(17)	0.012(2)	0.033	0.44169 (27)	1.53	0.321
Talampaya	0.7410	13.0	0.004(1)	0.041(2)	~0.02	0.168(8)	0.004(4)	0.005(1)	<0.001	0.14775 (38)	6.29	-
Diogenites												
Bilanga	1.0016	29.7	0.024(1)	0.023(1)	~0.05	0.091(5)	0.147(10)	0.002(1)	0.001	0.11764 (19)	0.415	0.086
Dhofar 700	0.5849	23.0	0.015(1)	0.026 (2)	~0.10	0.231(17)	0.191(19)	0.016 (2)	0.002	0.14144 (13)	5.14	-
Johnstown	0.8014	26.2	1.84(4)	1.73(4)	2.54(6)	3.41(7)	3.20(7)	0.193(4)	0.131	0.12208 (6)	0.503	0.083
Shalka	0.3717	25.8	0.054(2)	0.004(1)	0.005(4)	0.461(13)	0.004(4)	0.001(1)	0.003	0.11626 (72)	0.075	0.110
Tatahouine	1.0066	28.2	0.019(1)	0.015(1)	0.024(2)	0.044(3)	0.036(5)	0.004(1)	0.002	0.13095 (16)	0.872	0.062
dupl.	0.9062	-	0.015(0)	0.022(1)	-	0.093(7)	-	0.003(1)	0.001	0.13216 (19)	0.913	0.060
Olivine diogenites												
NWA 1877	0.1286	-	0.001(1)	<0.001	-	0.014(12)	-	0.008 (3)	<0.001	0.20417 (67)	33.6	-
NWA 2629	0.4904	-	0.010(1)	0.013 (2)	-	0.042(14)	0.028(10)	0.005 (1)	0.001	0.12743 (21)	2.51	-
Anomalous eucrites												
Ibitira	0.4212	7.6	0.018(1)	0.019(1)	0.029(4)	-	0.018(15)	<0.001	0.002	0.12795 (18)	0.132	0.118
Pasamonte	0.7123	6.5	0.424(9)	0.629(41)	1.33(12)	1.69(4)	1.29(7)	0.054(2)	0.034	0.12562 (6)	0.616	0.077
Dhofar 007	0.5421	-	57.3(50)	68.3(95)	75.9(90)	93.2(21)	64.8(15)	4.24(9)	5.01	0.12826 (1)	0.356	0.100
- metal$^{\beta}$	0.00127	-	3473(65)	3205(110)	4785(780)	6367(910)	6356(900)	280(40)	315	0.12951 (5)	0.388	0.100
SNCs												
Chassigny	0.1528	31.6	0.568(16)	0.637(22)	-	2.53(7)	0.25(11)	0.021(3)	0.028	0.12403 (11)	0.177	0.120
Nakhla	0.2075	12.1	0.037(3)	0.053(6)	0.190(35)	2.73(19)	1.27(16)	0.022(3)	0.017	0.16681 (17)	2.92	0.103
Shergotty	0.1556	9.5	0.441(13)	0.693(98)	1.98(51)	42.3(5.8)	61.3(11)	0.093(9)	0.015	0.12757 (5)	1.02	0.125
Zagami	0.1413	12.5	0.060(4)	0.037(6)	0.247(52)	6.7(5)	4.4(10)	0.033(4)	0.130	0.15868 (13)	2.65	0.151
Angrites												
D'Orbigny	0.1780	6.5	0.947(18)	1.09(3)	1.47(4)	2.72(7)	1.78(15)	0.045(3)	0.06	0.11909 (11)	0.227	0.101
NWA 2999	0.1619	-	206(4)	211(5)	333(13)	371(8)	238(5)	17.4(4)	18.0	0.12831 (8)	0.408	0.096
Sahara99555	0.1181	7.0	0.055(3)	0.107(8)	0.246(27)	1.37(5)	0.36(15)	1.78(13)	0.017	0.21080 (17)	157	-
Reference materials$^{\gamma}$												
TDB-1	1.01	-	0.104	0.059	0.188	4.63	24.7	-		0.9688 (3)	41.5	
TDB-1	1.00	-	0.120	0.063	0.195	4.92	22.5	-		0.9359 (9)	36.3	
TDB-1	1.01	-	0.117	0.067	0.206	4.89	24.5	-		0.9076 (3)	39.8	
TDB-1	1.00	-	-	0.061	0.251	5.82	21.9	0.98		-	-	
TDB-1	1.00	-	0.094	0.056	0.258	4.43	21.5	1.00		1.0531 (3)	57.8	
TDB-1	1.00	-	0.103	0.059	0.296	4.65	22.4	1.07		0.9733 (4)	55.2	
TDB-1	1.00	-	0.100	0.050	0.221	3.86	18.9	1.00		1.0633 (2)	53.9	

NOTES:

Re* - concentration estimated from $^{187}Os/^{188}Os$ composition and age, assuming chondritic initial.

* - Initial $^{187}Os/^{188}Os$ corrected for ingrowth of ^{187}Os.

- The deviation of the initial $^{187}Os/^{188}Os$ from the O-chondrite evolution curve: $((^{187}Os/^{188}Os_i/^{187}Os/^{188}Os_{chondrite})-1)*100$. Present day chondrite: $^{187}Os/^{188}Os = 0.1283$, $^{187}Re/^{188}Os = 0.422$ (*76*).

$^{\beta}$ – hand-picked separate metal fraction from Dhofar 007

$^{\gamma}$ – TDB-1 is a CANMET doleritic reference material.

The greatest sources of uncertainty in low-level measurements are powder heterogeneity and blank composition. Blank composition (and standard deviation) is given in Methods, although the total uncertainty quoted for the blank composition is overestimated as it includes analyses from different analytical sessions, using different reagent batches. The precise uncertainty on the blank is therefore difficult to estimate. The limited sample material available did not allow for numerous replicate analyses, but repeat analyses of the reference material TDB-1 gave uncertainties typically of the order of: 7% for Re concentration, 17-25% for Os, Ir, Pt and Pd and 34% for Ru.

MgO data from refs. (*50, 56, 66, 77, 78*)

	Os	Ir	Ru	Pt	Pd	Re
Metal/silicate low-P	10^{10}	$> 10^{12}$	10^{12}	10^{8} - 10^{15}	10^{7}	10^{10}
Metal/silicate high-P	10^{6} - 10^{8}	10^{7}	-	10^{3} – 10^{9}	300 – 10^{6}	200-440

Table S2. Range of metal-silicate partition coefficients (D) at low- and high-pressure conditions. Lowest available D values used for calculations to cover the range of possibilities, but due to the potential for sampling micro-nuggets formed in experimental work with HSE, the true values are more likely to match the highest values. References: (*1, 2, 7, 9-11, 27, 79-85*).